Electrochemically Induced Insertion of Ruthenium Atoms into a C–C Bond: Reversible Slicing of a Cyclooctatetraene Ligand†

William E. Geiger,*,‡ Albrecht Salzer,§ Joseph Edwin,‡ Wolfgang von Philipsborn,⊥ Umberto Piantini,⊥ and Arnold L. Rheingold∥

Contribution from the Department of Chemistry, University of Vermont, Burlington, Vermont 05405, Anorganisch-chemisches Institut der Universitat Zurich, CH-8057 Zurich, Switzerland, Organisch-chemisches Institut der Universitat Zurich, CH-8057 Zurich, Switzerland, and Department of Chemistry, University of Delaware, Newark, Delaware 19711.
Received March 22, 1990

Abstract: Oxidation of the pseudo-triple-decker complex $Cp_2Ru_2(\mu\text{-cyclo-}C_8H_8)$ (**1**) proceeds by a two-electron process at ambient temperatures to give the stable dication $Cp_2Ru_2(\mu\text{-cat-}C_8H_8)^{2+}$ (**2**). Whereas the bridging C_8H_8 moiety of **1** is a cyclooctatetraene ring, the C_8H_8 group in **2** is an open chain, so that the dication is a "flyover" complex. Insertion of both metal atoms into a C–C bond of the cyclooctatetraene is thus observed as a consequence of the redox process. The flyover dication is efficiently reduced back to the original complex **1**. Thus, **1** and **2** form a chemically reversible couple in which two-electron transfer leads to insertion and deinsertion of two metals into a C–C bond. The overall process is similar to those suggested regarding the metal-catalyzed cyclooligomerization of alkynes. The mechanism of the reaction has been studied by cyclic voltammetry, bulk coulometry, and other electrochemical methods. At low temperatures the two-electron oxidation wave of **1** becomes a one-electron wave owing to the stability of $\mathbf{1}^+$. At higher temperatures $\mathbf{1}^+$ isomerizes to the flyover monocation, which is then oxidized to **2**. The lifetime of $\mathbf{1}^+$ is ca. 50 ms at 263 K. The overall mechanism for the reaction $\mathbf{1} \rightleftharpoons \mathbf{2} + 2e^-$ appears to follow an ECE–EEC route. ^1H and ^{13}C NMR spectra of **2** were analyzed in terms of the flyover structure. Complex **1** is fluxional and was found to exhibit a rearrangement mechanism of clockwise 1,3-metal shifts of one of the Ru atoms on the cyclooctatetraene ring. This is identical with that observed earlier for the isoelectronic $Cp_2Rh_2(\mu\text{-}C_8H_8)^{2+}$, but the activation barrier is higher by ca. 1.4 kcal/mol at 320 K. The X-ray crystallographic structures of **1** and **2** have been determined: **1**, $Cp_2Ru_2(\mu\text{-cyclo-}C_8H_8)$, monoclinic, $C2/c$, $a = 13.880$ (4) Å, $b = 6.289$ (1) Å, $c = 16.514$ (4) Å, $\beta = 95.50$ (2)°, $V = 1435.0$ (7) Å^3, $Z = 4$, $R(F) = 2.51\%$; for **2**, $[Cp_2Ru_2(\mu\text{-cat-}C_8H_8)][PF_6]_2 0.5C_6H_6$, triclinic, $P\bar{1}$, $a = 9.237$ (3) Å, $b = 9.234$ (3) Å, $c = 16.151$ (5) Å, $\alpha = 80.31$ (3)°, $\beta = 74.09$ (2)°, $\gamma = 68.09$ (2)°, $V = 1225.8$ (7) Å^3, $Z = 2$, $R(F) = 3.89\%$.

Introduction

Beginning with the Reppe hypothesis[1] that a mononuclear nickelacycle plays a role in the nickel-catalyzed cyclotrimerization of acetylene, support has gathered for mono- and dimetallacycles as intermediates in metal-catalyzed oligomerizations of alkynes. Key reactions in a stepwise or "zipper"-type oligomerization mechanism are the insertion of one or more metals into a C–C bond (eq 1) and the elimination of the metal(s) from the modified linkage (eq 2).[2]

$$C\text{–}C' + M_n \rightarrow C\text{–}M_n\text{–}C' \qquad n = 1, 2 \qquad (1)$$

$$C\text{–}M_n\text{–}C'' \rightarrow C\text{–}C'' + M_n \qquad (2)$$

There is considerable interest in the preparation of model compounds which mimic this behavior.[2-8] Especially pertinent to the cyclooctatetraene case are two recent studies in which intramolecular rearrangements allow the oxidative addition reaction of eq 1 and/or the reductive elimination reaction of eq 2 to proceed with reasonably high efficiency. One involves a thermally induced reductive elimination reaction in which a linear C_8H_8 bridging ligand is converted to a bridging cyclooctatetraene ligand. Heating the flyover complex $Cp_2Cr_2(\mu\text{-cat-}C_8H_8)$, **3**, for 170 h at 450 K resulted in cleavage of the two Cr–C σ bonds and formation of the isomeric cyclooctatetraene complex **4** in 50% yield.[8]

The second study, reported as a brief communication,[9] involves high-yield electron-transfer-induced interconversion of **1** and **2**. Thus, oxidation of the pseudo-triple-decker complex $Cp_2Ru_2(\mu\text{-cyclo-}C_8H_8)$, **1**, results in the flyover dication $[Cp_2Ru_2(\mu\text{-cat-}C_8H_8)]^{2+}$, **2**. Electrochemical reduction of **2** reforms **1**. We now report details of this redox chemistry, which represents a remarkably rapid and efficient example of an oxidative addition reaction (eq 1) and reductive elimination reaction (eq 2) facilitated by electron-transfer processes.

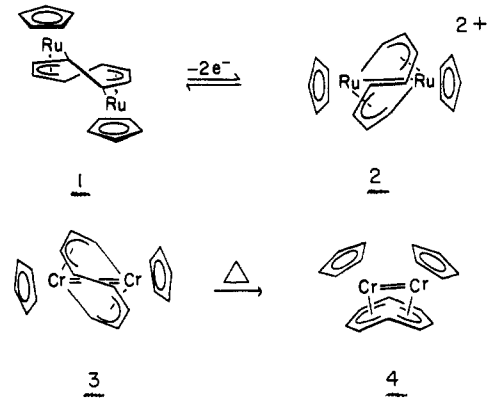

Variable-temperature voltammetry experiments show that the structural change from the pseudo-triple-decker structure of **1** to the flyover structure of **2** occurs in the *monocation* intermediate,

† Part 22 of the series *Structural Consequences of Electron-Transfer Reactions*. Part 21: Edwin, J.; Geiger, W. E., preceding article in this issue.
‡ University of Vermont.
§ Anorganisch-chemisches Institut der Universitat Zurich.
⊥ Organisch-chemisches Institut der Universitat Zurich.
∥ University of Delaware.

(1) (a) Reppe, W.; Schlichting, O.; Klager, K.; Toepel, T. *Justus Liebigs Ann. Chem.* **1948**, *560*, 1. (b) Reppe, W.; Vetter, H. *Ibid.* **1953**, *582*, 133.
(2) (a) Wilke, G. *Pure Appl. Chem.* **1978**, *50*, 677. Wilke, G. *Angew. Chem., Int. Ed. Engl.* **1988**, *27*, 185.
(3) (a) Knox, S. A. R.; Stansfield, R. F. D.; Stone, F. G. A.; Winter, M. J.; Woodward, P. *J. Chem. Soc., Chem. Commun.* **1978**, 221. (b) Green, M.; Norman, N. C.; Orpen, A. G. *J. Am. Chem. Soc.* **1981**, *103*, 1269.
(4) Colborn, R. E.; Vollhardt, K. P. C. *J. Am. Chem. Soc.* **1981**, *103*, 6259 and references therein.
(5) (a) Eisch, J. J.; Piotrowski, A. M.; Han, K. I.; Kruger, C.; Tsay, Y. H. *Organometallics* **1985**, *4*, 224. (b) Eisch, J. J.; Galle, J. E.; Aradi, A. A.; Boleslawski, M. P. *J. Organomet. Chem.* **1986**, *312*, 399.
(6) Yur'eva, L. P. *Russ. Chem. Rev.* **1974**, *43*, 48.
(7) Lawrie, C. J.; Gable, K. P.; Carpenter, B. K. *Organometallics* **1989**, *8*, 2274.
(8) (a) Heck, J.; Rist, G. *J. Organomet. Chem.* **1988**, *342*, 45. (b) Elschenbroich, C.; Heck, J.; Massa, W.; Schmidt, R. *Angew. Chem., Int. Ed. Engl.* **1983**, *22*, 330.
(9) Edwin, J.; Geiger, W. E.; Salzer, A.; Ruppli, U.; Rheingold, A. L. *J. Am. Chem. Soc.* **1987**, *109*, 7893.

0002-7863/90/1512-7113$02.50/0

so that **2** is formed from **1** through an ECE mechanism.[10] The two-electron reduction of **2** reforming **1** appears to go through an EEC process. This paper presents details of the electrochemical interconversion of eq 3, aspects of the NMR behavior of both redox partners, and a comparison of their structures.

$$\mathbf{1} \rightleftharpoons \mathbf{2} + 2e^- \quad (3)$$

Experimental Section

Chemicals. The following compounds were prepared by literature methods: $[Cp_2Rh_2(\mu\text{-cyclo-}C_8H_8)][PF_6]_2$,[11] **5**$[PF_6]_2$, $Cp_2Ru_2(\mu\text{-cyclo-}C_8H_8)$,[12] **1**, and $[Cp^*Ni(\eta^4\text{-}C_8H_{12})][BF_4]$.[13] All chemical and electrochemical experiments were conducted under an atmosphere of prepurified nitrogen which had been further treated by drying with molecular sieves and deoxygenating with a copper-based catalyst. Standard Schlenck procedures were employed. All reagent solvents were freshly distilled from drying agents, and NMR solvents were dried over type 3A molecular sieves.

Preparation of $[Cp_2Ru_2(\mu\text{-cat-}C_8H_8)][PF_6]_2$, $[2][PF_6]_2$. (a) Through Chemical Oxidation by Ferrocenium in CH_2Cl_2 at 298 K. Three hundred fifty milligrams (0.802 mmol) of $Cp_2Ru_2(\mu\text{-cyclo-}C_8H_8)$, **1**, and 500 mg (1.51 mmol) of $[Cp_2Fe][PF_6]$ were stirred in 10 mL of CH_2Cl_2 for 1 h. After removal of CH_2Cl_2, the residue was washed with diethyl ether until free of ferrocene, dissolved in acetone (5 mL), and precipitated with ether. The brown precipitate was washed several times with small amounts of CH_2Cl_2. The dichloromethane washings contained the mononuclear byproduct $CpRu(\eta^6\text{-}C_8H_8)^+$, identified by its NMR spectrum. The brown CH_2Cl_2-insoluble crystals were dried under vacuum. X-ray and analytical grade crystals were grown by filtering 3 mL of a CH_3NO_2 solution through a 2-mm layer of activity 1 neutral alumina over a fine frit, then concentrating the solution to about 1 mL, and vapor diffusing benzene into it over 24 h. The crystals were identified as $[2][PF_6]_2 \cdot {}^1/_2C_6H_6$ by NMR and X-ray analyses. Yields of pure **2** were 150–300 mg (20–40%). Elemental anal. (Robertson Laboratories) Calcd for $C_{21}H_{21}F_6PRu_2$: C, 32.95; H, 2.77. Found: C, 33.03; H, 2.62.

(b) Through Electrochemical Oxidation in CH_2Cl_2 at 218 K. Thirty-eight milligrams (0.087 mmol) of **1** was dissolved in 50 mL of CH_2Cl_2/0.1 M Bu_4NPF_6 to make a 1.74 mM solution. The temperature was lowered to 218 K, and the complex was electrolyzed at +0.25 V, a potential just positive of the one-electron oxidation wave of **1** at this temperature (vide infra). The electrolysis proceeded slowly at a Pt basket working electrode, reaching 98% completion in about 2 h. The Coulomb count showed that 1.9 F of electricity were released per mol of **1**. Buff-colored microcrystals appeared as the reaction proceeded. After electrolysis there were no major waves in CV scans of the solution. The electrolysis solution was transferred to a flask and kept at 240 K for 2 days, after which the supernate was removed by syringe, and the crystals were washed several times with CH_2Cl_2. After the crystals were vacuum dried, a yield of 50 mg (88%) was obtained. The crystals were shown to be pure $[2][PF_6]_2$ by NMR spectroscopy.

Electrochemistry. Electrochemical procedures were essentially as given in the preceding paper in this issue. Potentials are reported versus the aqueous S.C.E., against which Cp_2Fe/Cp_2Fe^+ has an $E°$ of +0.46 V (CH_2Cl_2/0.1 M Bu_4NPF_6) or +0.48 V (acetone/0.1 M Bu_4NPF_6). Pt was used as the working electrode both in voltammetry and coulometry experiments. Some voltammetry scans were also performed at a gold electrode, and no differences in redox behavior were detected.

NMR Spectroscopy. ^1H and ^{13}C spectra were recorded at 400 and 100 MHz, respectively, on a Bruker AM-400 FT-NMR spectrometer. Typical acquisition parameters were as follows: ^1H, spectral width (SW), 8000 Hz; number of spectral data points (SI), 32 K; pulse angle (PW), 9 μS; acquisition time (AQ), 3.2 s; relaxation delay (RD), 0.0 s; ^{13}C, SW = 20000 Hz, SI = 64 K, PW = 13.5 μs, AQ = 0.6 s, RD = 2.5 s. Chemical shifts are given in units of δ (ppm).

Single-Crystal X-ray Diffraction Studies of 1, 2, and 5. The parameters used during collection of diffraction data for **1**, **2**, and **5** are summarized in Table I. The crystal structures were determined at the University of Delaware. The crystals were mounted on glass fibers with epoxy cement.

A red crystal of **2** was found to have no symmetry higher than triclinic, space group $P\bar{1}$ (the presence of inversional symmetry in the lattice confined work to the centrosymmetric alternative). The unit-cell parameters were obtained from the angular setting of 25 reflections ($20° \le 2\theta \le 25°$). The structure was solved by direct methods which located the metal atoms. The remaining non-hydrogen atoms were located through subsequent difference Fourier and least-squares synthesis. All non-hydrogen atoms were refined anisotropically. All hydrogen atoms, except those of a half molecule of benzene, were found and refined isotropically. The benzene hydrogen atoms were incorporated as idealized contributions [d(CH) = 0.96 Å]. All computer programs and sources of neutral atom scattering factors for this and the following structure are contained in SHELXTL (5.1) library (Sheldrick, G. Nicolet XRD, Madison, WI).

A crystal of **1** was found from systematic absences and photographic evidence to crystallize in either of the monoclinic space groups $C2/c$ or Cc. The former was initially chosen based on E statistics and subsequently verified by the results of refinement. Unit cell parameters were obtained as for **2**. The structure was solved by direct methods which located a Ru atom. The remaining atoms were located from subsequent difference Fourier synthesis. All non-hydrogen atoms were refined anisotropically. The hydrogen atoms of the cyclooctatetraene ring were found and refined isotropically, while the hydrogen atoms of the Cp rings were incorporated as idealized contributions [d(CH) = 0.96 Å].

For **5**, systematic absences and photographic evidence were consistent with the orthorhombic space group $P2_12_12$. The unit cell parameters were obtained as for **2**. The structure was solved by using direct methods which located a Rh atom. All remaining non-hydrogen atoms were found through successive cycles of difference Fourier maps followed by least-squares refinement and were refined anisotropically. All hydrogen atoms were incorporated as idealized isotropic contributions. Since **5** is isostructural with **1**, structural details are not provided.[11]

Table I. Crystallographic Data

	2	**1**
	(a) Crystal Parameters	
formula	$[C_{18}H_{18}Ru_2][PF_6]_2 \cdot 0.5C_6H_6$	$(CpRu)_2(cot)$
space group	$P\bar{1}$	$C2/c$
crystal system	triclinic	monoclinic
a, Å	9.237 (3)	13.880 (4)
b, Å	9.234 (3)	6.289 (1)
c, Å	16.151 (5)	16.514 (4)
α, deg	80.31 (3)	
β, deg	74.09 (2)	95.50 (2)
γ, deg	68.09 (2)	
V, Å^3	1225.8 (7)	1435.0 (7)
Z	2	4
ρ(calcd), g cm^{-3}	2.074	2.020
temp, °C	20	22
μ, cm^{-1} (Mo Kα)	14.4	20.5
cryst dimens, mm	0.24 × 0.26 × 0.30	0.21 × 0.26 × 0.26
	(b) Data Collection	
diffractometer	Nicolet R3m	[a]
monochromator	graphite	[a]
radiation	Mo Kα (λ = 0.71073)	[a]
scan technique	Wyokoff	$\theta/2\theta$
2θ scan range, deg	4–55	4–55
data collected	$\pm h, \pm k, \pm l$	$\pm h, +k, +l$
scan speed, deg/min	variable, 7–20	variable, 6–20
rflns collected	5891	1853
independent data	5605	1645
independent data obsd	4558 ($3\sigma(F_o)$)	1459 ($3\sigma(F_o)$)
std reflns	3 std/197 rflns	3 std/197 rflns
var. in stds	~2%	<1%
	(c) Refinement	
$R(F)$, %	3.89	2.51
$R(wF)$, %	4.57	3.30
Δ/σ (max)	0.070	0.042
$\Delta(\rho)$, eÅ^{-3}	0.77	0.98
N_o/N_v	11.2	13.5
weighting factor, g ($\omega^{-1} = \sigma^2(F_o) + g(F_o)^2$)	0.001	0.001
GOF	1.440	1.237

[a] Same.

Results and Discussion

I. Electrochemistry. A. General Redox Behavior. $Cp_2Ru_2(\mu\text{-cyclo-}C_8H_8)$, **1**, gives an irreversible anodic wave twice the height of 1e$^-$ standards at room temperature and low CV scan rates (< 1 V/s) which is well-behaved in CH_2Cl_2 and acetone solutions. The neutral complex is easily soluble in both solvents, whereas the resulting dication **2** is much more soluble in acetone than in CH_2Cl_2. The basic flyover structure of **2** (Figure 10) with its *open* eight-carbon chain bridging the two metals was implied

(10) E symbolizes a heterogenous electron transfer. C symbolizes a chemical reaction, a structural rearrangement in the present case.

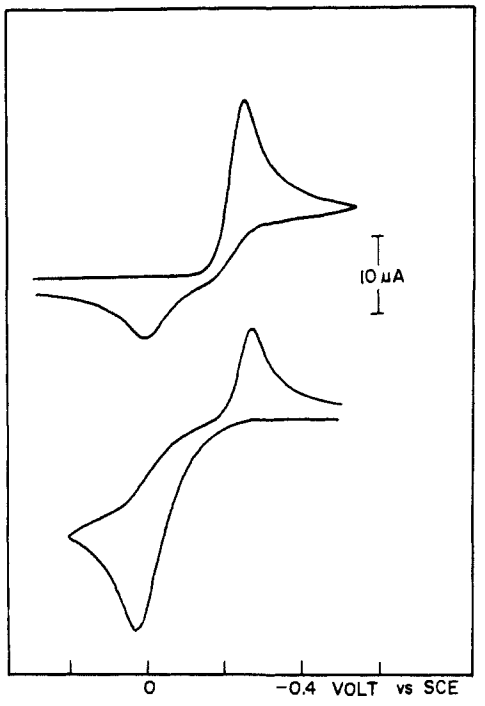

Figure 1. Cyclic voltammograms of **2** (top) and **1** (bottom). **1** (1.8 mM) in acetone was exhaustively electrolyzed to produce **2**. CV's taken before (bottom) and after (top) electrolysis. Conditions: Pt electrode; acetone/0.1 M Bu_4NPF_6; ambient temperatures; scan rate 0.064 v/s (top), 0.070 v/s (bottom).

by its NMR spectra (vide infra) and was established unequivocally by crystallography. Complex **2** displays an irreversible cathodic wave which results in reformation of complex **1** with its *cyclic* eight-carbon ring bridging the metal atoms. Therefore, **1** and **2** form the chemically reversible couple of eq 4. Chemical oxidation

$$\underset{\mathbf{1}}{Cp_2Ru_2(\mu\text{-cyclo-}C_8H_8)} \rightleftharpoons \underset{\mathbf{2}}{[Cp_2Ru_2(\mu\text{-cat-}C_8H_8)]^{2+}} + 2e^- \quad (4)$$

of **1** with Cp_2Fe^+ gives **2** in less than 50% yield, but high yields of **2** are obtained when **1** is electrolyzed at low temperatures. Electrolytic conversion of **2** back to **1** is virtually quantitative at ambient temperatures.

The oxidation of $Cp_2Ru_2(\mu\text{-cyclo-}C_8H_8)$ changes from a single two-electron CV wave at 298 K to a pair of one-electron processes at low temperatures. The monocation $Cp_2Ru_2(\mu\text{-cyclo-}C_8H_8)^+$ is thereby detected below 240 K, concomitant with a second wave for the irreversible one-electron oxidation of $Cp_2Ru_2(\mu\text{-cyclo-}C_8H_8)^+$ and a reversible couple arising from an unidentified reaction of the dication $Cp_2Ru_2(\mu\text{-cyclo-}C_8H_8)^{2+}$.

The formation of $Cp_2Ru_2(\mu\text{-cat-}C_8H_8)^{2+}$ from $Cp_2Ru_2(\mu\text{-cyclo-}C_8H_8)$ proceeds via an ECE process, in which the intervening chemical reaction is the isomerization of $\mathbf{1}^+$ to $Cp_2Ru_2(\mu\text{-cat-}C_8H_8)^+$. Reduction of $Cp_2Ru_2(\mu\text{-cat-}C_8H_8)^{2+}$ apparently gives **1** through an EEC process, with the isomerization (chain closing) occurring after formation of neutral $Cp_2Ru_2(\mu\text{-cat-}C_8H_8)$. The evidence follows.

I.B. Oxidation of $Cp_2Ru_2(\mu\text{-cyclo-}C_8H_8)$, 1. Cyclic Voltammetry. In CH_2Cl_2 or acetone, **1** has a diffusion-controlled but irreversible anodic wave of $2e^-$ height (twice that of a $1e^-$ standard, vide infra) with a peak potential of +0.02 V vs SCE (v = 0.1 V/s). On the reverse sweep a cathodic wave appears at E_{pc} = −0.26 V which is also irreversible and is due to reduction of **2** (Figure 1). Multiple cycle experiments show no new waves in this region. The anodic wave has a width ($E_p - E_{p/2}$) characteristic of a fast $1e^-$ transfer, and its two-electron height is due to an ECE process wherein the initially formed monocation $\mathbf{1}^+$ rearranges to a complex immediate oxidized by one more electron. This mechanism is strongly supported by CV experiments at subambient temperatures. Table II summarizes some voltammetry data for **1** and **2**.

The number of electrons transferred in the anodic wave was

Table II. Cyclic Voltammetry Data for $Cp_2Ru_2(\mu\text{-cyclo-}C_8H_8)$, **1**, and $[Cp_2Ru_2(\mu\text{-cat-}C_8H_8)]^{2+}$, **2**, at Pt Electrode, Potentials in V vs SCE

complex	solvent	T (K)	δE^a (mV)	E_{pa}	E_{pc}	$E°_{app}$	v (Vs^{-1})
1	CH_2Cl_2	298	58	+0.017	−0.257	−0.12	0.1
1	acetone	298	55	+0.02	−0.26	−0.12	0.1
2	acetone	298	45	+0.01	−0.27	−0.13	0.12
2	acetone	253	72		−0.48		0.1
2	acetone	204	105		−0.60		0.5

$^a\delta E = E_p - E_{p/2}$.

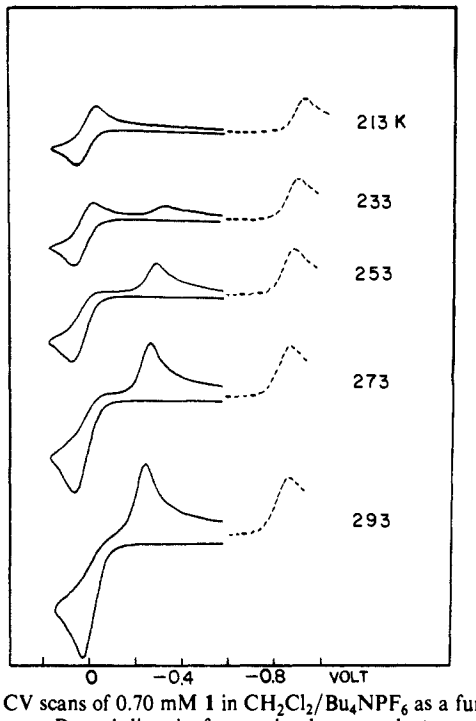

Figure 2. CV scans of 0.70 mM **1** in CH_2Cl_2/Bu_4NPF_6 as a function of temperature. Dotted line is for equimolar one-electron standard $[Cp^*Ni(\eta^4\text{-}C_8H_{12})]^+$, scan rate 0.20 V/s, Pt electrode; approximate peak current at 213 K was 1 μA. Actual reference was Ag wire quasi-reference, so potentials are referenced to the Ni(II) standard, assuming its $E°$ = −0.82 V vs SCE.

investigated as a function of temperature by comparison of the wave height with that of a one-electron internal standard. The nickel π complex $[Cp^*Ni(\eta^4\text{-}C_8H_{12})]^+$ was chosen because it is soluble in CH_2Cl_2 over a wide temperature range and gives a reversible one-electron reduction[14] at a potential sufficiently removed from **1** and **2** to avoid overlap. Its $E°$ at 298 K is −0.82 V vs SCE or −1.28 V vs $Cp_2Fe^{0/+}$.

Figure 2 shows that the mechanism of the oxidation of **1** changes as the temperature is lowered. At 293 K the ratio of the anodic peak height of **1** to the cathodic height of the $1e^-$ standard is 2.0. As the temperature is lowered, this ratio decreases (last column of Table III and Figure 3) until below 213 K it becomes 1.0.

When the temperature was such that the wave approached $1e^-$ height, it became reversible, with its ΔE_p and peak width matching those of the standard (Table III). At temperatures below about 243 K (Figure 2) the reverse scan shows that the formation of the flyover complex **2** is incomplete and that one-electron of **1** to $\mathbf{1}^+$ is favored. Equations 5–7 describe the ECE process accounting for these data. The current ratios from Table III and

$$Cp_2Ru_2(\mu\text{-cyclo-}C_8H_8) \rightleftharpoons Cp_2Ru_2(\mu\text{-cyclo-}C_8H_8)^+ + e^- \quad E°_{1,cy} \quad (5)$$

$$Cp_2Ru_2(\mu\text{-cyclo-}C_8H_8)^+ \xrightarrow{k^+_{isom}} Cp_2Ru_2(\mu\text{-cat-}C_8H_8)^+ \quad C \quad (6)$$

$$Cp_2Ru_2(\mu\text{-cat-}C_8H_8)^+ \rightleftharpoons Cp_2Ru_2(\mu\text{-cat-}C_8H_8)^{2+} + e^- \quad E°_{2,cat} \quad (7)$$

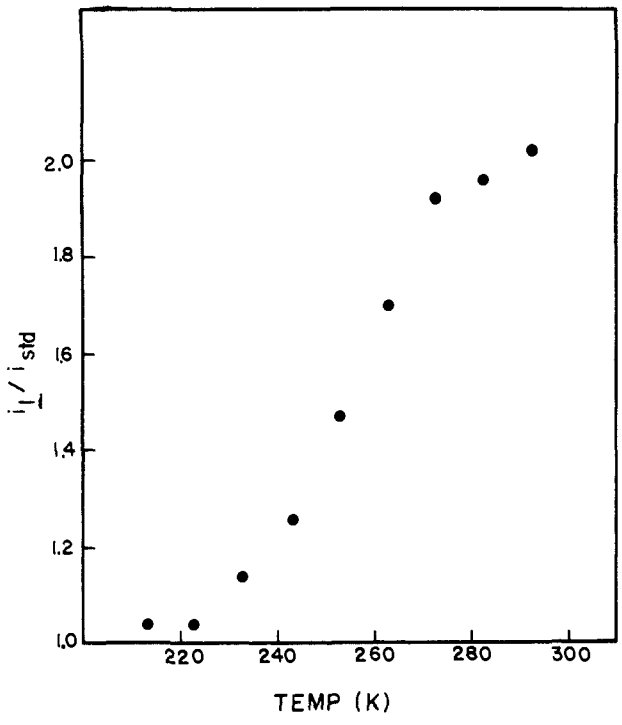

Figure 3. Temperature dependence of ratio of anodic peak height of **1** to cathodic peak height of Ni(II) one-electron standard. Data taken from scans like those in Figure 2.

Table III. Variable Temperature Cyclic Voltammetry Data for the Oxidation of $Cp_2Ru_2(\mu\text{-cyclo-}C_8H_8)$, **1**, in CH_2Cl_2 at a Pt Electrode, Compared to the One-Electron Standard $[Cp^*Ni(\eta^4\text{-}C_8H_{12})]^+$ [b]

T (K)	δE^a(1) (mV)	E_{pa}(1)	i_{pa}(1) (μA)	δE(std) (mV)	i_{pc}(std) (μA)	i_1/i_{std}
293	60	+0.025	2.35	60	1.16	2.02
283	62	+0.03	2.25	62	1.15	1.96
273	60	+0.05	2.00	60	1.04	1.92
263	60	+0.06	1.70	58	1.00	1.70
253	60	+0.06	1.40	58	0.95	1.47
243	58	+0.06	1.15	54	0.91	1.26
233	54	+0.05	1.00	54	0.88	1.14
223	54	+0.05	0.88	54	0.82	1.04
213	52	+0.06	0.78	54	0.75	1.04

[a] $\delta E = E_p - E_{p/2}$. [b] Potentials in V vs SCE. The concentration of each compound was 7.0×10^{-4} M.

Figure 3 were used along with the method of Nicholson[15] to calculate the rate constant k^+_{isom} of the isomerization reaction of eq 6, i.e., the chain-opening reaction. As detailed in Table IV, the half-life of the pseudo-triple-decker monocation $[Cp_2Ru_2(\mu\text{-cyclo-}C_8H_8)]^+$, $\mathbf{1}^+$, is less than 1 s at $T > 230$ K.

The ECE scheme of eqs 5–7 requires that $E^\circ_{2,cat} \leq E^\circ_{1,cy}$, so that the flyover monocation $Cp_2Ru_2(\mu\text{-cat-}C_8H_8)^+$ immediately oxidizes to the dication **2**. At high temperatures k^+_{isom} is fast, and the ECE process goes to completion within the CV scan time. This scheme also requires that the *flyover* structure is thermodynamically favored in the monocation. Supporting this mechanism, the reduction wave at −0.3 V for the flyover dication **2** is visible on reverse sweeps only when $\mathbf{1}^+$ has had sufficient time to rearrange to the flyover structure (Figure 2).

When $\mathbf{1}^+$ is stable, e.g., at low temperatures, a second oxidation wave is expected for the process $\mathbf{1}^+/\mathbf{1}^{2+}$, since pseudo-triple-decker complexes generally have accessible dications.[9,16,17] Therefore eq 8 appears to account for peak B in Figure 4 which grows in at

$$\mathbf{1}^+ \rightleftharpoons \mathbf{1}^{2+} + e^- \qquad E^\circ_{2,cy} \tag{8}$$

low temperatures. Its potential, ca. +0.3 to 0.4 V, is measurable only over a short temperature span. It does not appear to separate from the first wave as the temperature is lowered, as found for the dirhodium analogue,[17] since the shape of the first wave does

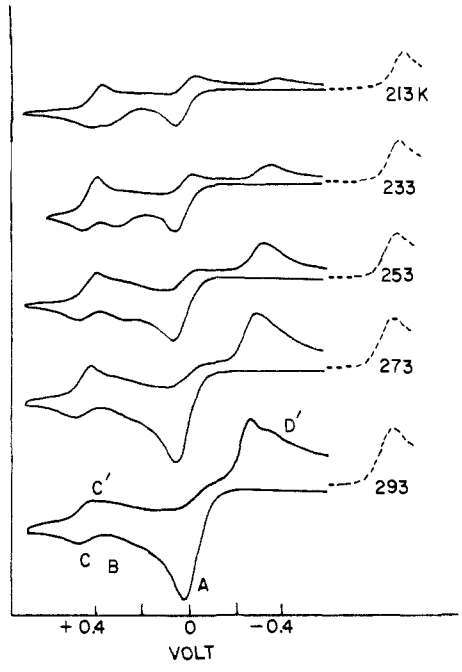

Figure 4. CV scans of same solution as Figure 2 [0.70 mM **1** and Ni(II) standard] as function of temperature over wider potential range. Peak assignments: A, oxidation of **1** (eq 14); B, oxidation of $Cp_2Ru_2(\mu\text{-cyclo-}C_8H_8)^+$ (eq 16); C and C′ as well as D′ are from the unidentified product of reaction of dication of $Cp_2Ru_2(\mu\text{-cyclo-}C_8H_8)$, E°values of +0.46 V and −0.29 V; cathodic feature just negative of −0.2 V is due to reduction of **2**.

not appreciably change as the temperature is lowered. Therefore it appears that, unless the overpotential of the couple $\mathbf{1}^+/\mathbf{1}^{2+}$ is very high, $E^\circ_{2,cy} > E^\circ_{1,cy}$. However, since $E^\circ_{2,cy}$ is close to $E^\circ_{1,cy}$, the possible role of disproportionation of $\mathbf{1}^+$ in the formation of **2**, through eqs 9 and 10, was considered.

$$2\mathbf{1}^+ \rightleftharpoons \mathbf{1} + \mathbf{1}^{2+} \tag{9}$$

$$\mathbf{1}^{2+} \rightarrow \mathbf{2} \tag{10}$$

The temperature (233 K) and scan rate (0.2 V/s) of this experiment were chosen so that the lifetime of $\mathbf{1}^+$ was similar to the scan time between the waves of **1** and **2**. Over the concentration range of 0.35 to 2.2 mM, the wave for **2** did not increase relative to **1**, nor did the i_c/i_a value decrease for $\mathbf{1}/\mathbf{1}^+$. Thus concentration had no effect on the rate of appearance of **2** nor on the rate of disappearance of $\mathbf{1}^+$. The implication is that eq 10 (metal insertion at the dication stage) is *not* responsible for flyover formation, lending further credence to the ECE mechanism of eqs 5–7.

Scanning through the *second* oxidation wave of **1** (wave B in Figure 4) results in two *new* reversible couples apparently due to a single unidentified species. The couple with E° = +0.46 V is evident as waves C and C′ of Figure 4. The other couple at E° = −0.29 V has a cathodic branch (peak D′, Figure 4) which overlaps in position with that of **2**. Figure 5 shows most clearly that these two new couples grow in when multiple cycles are scanned through wave B ($\mathbf{1}^+/\mathbf{1}^{2+}$) at low temperatures. These scans are significant because they indicate that the oxidation of **1** to its *dication* does *not* lead to the flyover dication **2**. Rather, another complex of unspecified structure is formed. Chemical

(11) Edwin, J.; Geiger, W. E.; Rheingold, A. L. *J. Am. Chem. Soc.* **1984**, *106*, 3052. Details available from Dr. A. L. Rheingold at University of Delaware.
(12) Bieri, J. H.; Egolf, T.; von Philipsborn, W.; Piantini, U.; Prewo, R.; Ruppli, U.; Salzer, A. *Organometallics* **1986**, *5*, 2413.
(13) Koelle, U.; Fuss, B.; Khouzami, F.; Gersdorf, J. *J. Organomet. Chem.* **1985**, *290*, 77. This complex was also prepared by the reaction of cod with $[Cp_2Ni_2(\mu\text{-}C_2Ph_2)]^+$, results to be published.
(14) Edwin, J., unpublished work, University of Vermont.
(15) Nicholson, R.; Shain, I. *Anal. Chem.* **1965**, *37*, 179 and 190.
(16) Moraczewski, J.; Geiger, W. E. *J. Am. Chem. Soc.* **1978**, *100*, 7429.
(17) Preceding paper in this issue.

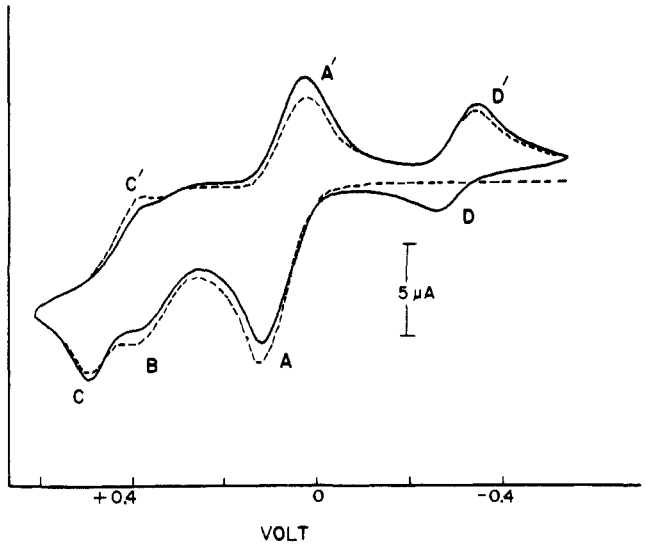

Figure 5. Multiple cycle CV scans of 0.69 mM **1** in CH_2Cl_2/Bu_4NPF_6 at 212 K, Pt electrode, scan rate 0.20 V/s. Dotted line refers to first scan, solid line to steady-state curve (fifth cycle and beyond). Peak assignments are as in Figure 4, with reversible couples designated by normal and primed letters.

oxidations in CH_2Cl_2 or acetone with 2 equiv of Cp_2Fe^+ below 240 K gave parallel results: the dominant products are the unidentified complex and $CpRu(\eta^6\text{-}C_8H_8)^+$.[18]

Bulk Electrolyses. Bulk coulometry of 1.9 mM **1** in acetone at 298 K with $E_{appl} = +0.25$ V confirmed the two-electron process of eq 3 (1.93 F measured for 98% complete electrolysis). The primary waves after electrolysis were those of **2** ($E_{pc} = -0.26$ V, $E_{pa} = +0.02$ V) and $CpRu(\eta^6\text{-}C_8H_8)^+$ ($E_{pc} = -1.0$ V). Back-electrolysis with $E_{appl} = -0.5$ V passed 1.0 F and regenerated **1** in 50% overall yield.

Low-temperature electrolysis greatly increased the yield of the flyover complex. The buff-colored precipitate of **2** appeared over 2 h as 1.7 mM **1** was electrolyzed in CH_2Cl_2 at 218 K with $E_{appl} = +0.25$ V. At completion, 1.9 F had passed, and CV scans showed only minor waves for **2** (owing to its low solubility at this temperature) and $CpRu(\eta^6\text{-}C_8H_8)^+$. Isolation of this precipitate gave 88% of apparently pure $[Cp_2Ru_2(\mu\text{-cat-}C_8H_8)]^{2+}$.

I.C. Reduction of $[Cp_2Ru_2(\mu\text{-cat-}C_8H_8)]^{2+}$, 2. The cathodic wave for $[Cp_2Ru_2(\mu\text{-cat-}C_8H_8)]^{2+}$, **2**, is diffusion controlled over the scan rate range of 0.04–0.50 V/s with a coupled anodic wave at +0.01 V. The cathodic wave half-width was 43–48 mV, and its peak potential moved negatively by 38 mV (uncorrected for IR loss) over this range. These data are consistent with a two-electron reduction for **2** with quasi-reversible charge-transfer kinetics. A rotating Pt electrode scan of the cathodic wave had a slope of $-E_{app}$ vs. log $[i/(i_d - i)]$ of 34 mV, also consistent with this picture. Bulk electrolysis of **2** at ambient temperatures gave virtually quantitative yields of the pseudo-triple-decker complex **1**.

At reduced temperatures the cathodic wave broadened considerably and moved steadily to more negative potentials. Reversibility was not observed even at 203 K, in contrast to the low-temperature scans of the oxidation wave (vide ante). A scheme that is consistent with this data is an EEC mechanism, eqs 11–13.

$$Cp_2Ru_2(\mu\text{-cat-}C_8H_8)^{2+} + e^- \rightleftharpoons Cp_2Ru_2(\mu\text{-cat-}C_8H_8)^+ \quad E^\circ_{2,cat} \quad (11)$$

$$Cp_2Ru_2(\mu\text{-cat-}C_8H_8)^+ + e^- \rightleftharpoons Cp_2Ru_2(\mu\text{-cat-}C_8H_8) \quad E^\circ_{1,cat} \quad (12)$$

$$Cp_2Ru_2(\mu\text{-cat-}C_8H_8) \rightarrow Cp_2Ru_2(\mu\text{-cyclo-}C_8H_8) \quad C \quad (13)$$

(18) Gill, T. P.; Mann, K. R. *Organometallics* **1982**, *1*, 485. An authentic sample of this complex had an irreversible reduction wave at −1.02 V vs SCE in acetone and −0.98 V in CH_2Cl_2.

Scheme I

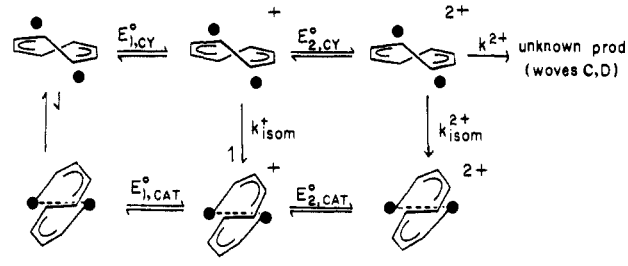

Although these data do not rule out the possibility of an ECE mechanism, the fact that the flyover structure is thermodynamically favored for both the dication and the monocation makes it very likely that the isomerization occurs after the second electron transfer in this case.

I.D. The Overall Redox Mechanism. The oxidation–reduction cycle **1** ⇌ **2** + 2e⁻ therefore consists of the six-step ECE–EEC process[19] (eqs 14–19 and Scheme I, where the rate constant for eq 15 refers to $T > 273$ K).

Oxidation

$$Cp_2Ru_2(\mu\text{-cyclo-}C_8H_8) \rightleftharpoons Cp_2Ru_2(\mu\text{-cyclo-}C_8H_8)^+ \quad E^\circ_{1,cy} \quad (14)$$
(**1**)

$$Cp_2Ru_2(\mu\text{-cyclo-}C_8H_8)^+ \rightarrow Cp_2Ru_2(\mu\text{-cat-}C_8H_8)^+ \quad k^+ > 28\ s^{-1} \quad (15)$$

$$Cp_2Ru_2(\mu\text{-cat-}C_8H_8)^+ \rightleftharpoons Cp_2Ru_2(\mu\text{-cat-}C_8H_8)^{2+} \quad E^\circ_{2,cat} \quad (16)$$
(**2**)

Reduction

$$Cp_2Ru_2(\mu\text{-cat-}C_8H_8)^{2+} \rightleftharpoons Cp_2Ru_2(\mu\text{-cat-}C_8H_8)^+ \quad E^\circ_{2,cat} \quad (17)$$
(**2**)

$$Cp_2Ru_2(\mu\text{-cat-}C_8H_8)^+ \rightleftharpoons Cp_2Ru_2(\mu\text{-cat-}C_8H_8) \quad E^\circ_{1,cat} \quad (18)$$

$$Cp_2Ru_2(\mu\text{-cat-}C_8H_8) \rightarrow Cp_2Ru_2(\mu\text{-cyclo-}C_8H_8) \quad \text{fast} \quad (19)$$
(**1**)

The overall two-electron process therefore appears to follow a route found recently for several other chemically reversible two-electron processes:[20] sequential one-electron processes in which either the first or second electron transfer creates an unstable isomer, leading to rapid rearrangements. If only the forward and reverse voltammetric peaks of the overall reaction are observed, it is generally not possible to distinguish between ECE and EEC sequences. In the present case, however, the low-temperature experiments show that the *cyclo* to *open* (*catena*) chain isomerization occurs after the *first* electron transfer in the oxidation step, allowing diagnosis of the sequence of electron transfers and structural rearrangements.

I.E. High-Temperature Voltammetry of ⇌ 2 + 2e⁻. If all the reactions of Scheme I were rapid and reversible, the voltammetric behavior of the reaction **1** ⇌ **2** + 2e⁻ would be Nernstian.[21] Although this might appear to be an unlikely possibility given the structural changes involved, we found that CV scans at elevated temperatures gave wave shapes close to those expected for fully reversible (Nernstian) electron transfers. DMSO was chosen as solvent owing to its high boiling point.

In CV scans at $v = 0.05$–0.3 V/s, the ΔE_p value decreased steadily as the temperature was raised, in response to acceleration

(19) This analysis does not take into account homogeneous electron-transfer processes (cross reactions) which may further complicate the treatment. See: Evans, D. H.; O'Connell, K. M. In *Electroanalytical Chemistry*; Bard, A. J., Ed.; Marcel Dekker: New York, 1986; Vol. 14.

(20) Examples of ECE/EEC processes have been given as refs 45–54 in ref 17.

(21) Geiger, W. E. In *Progress in Inorganic Chemistry*; Lippard, S. J., Ed.; John Wiley and Sons: New York, 1985; Vol. 33, p 275.

Table IV. Half-Lives of $[Cp_2Ru_2(\mu\text{-cyclo-}C_8H_8)]^+$, 1^+, in CH_2Cl_2 at Various Temperatures as Measured by Cyclic Voltammetry[a]

T (K)	i_l/i_{std}[b]	k (s^{-1})	$t_{1/2}$ (s)
273	1.92	28.0	0.025
263	1.70	12.7	0.05
253	1.47	4.6	0.15
243	1.26	1.9	0.36
233	1.14	0.85	0.81

[a] The ratio i_l/i_{std} is taken to be the number of electrons transferred in the ECE oxidation of **1**. It is used as the value of X_k/X_d in the calculation of the decomposition rate constant of 1^+, by using the following theory: Nicholson, R. S.; Shain, I. *Anal. Chem.* **1964**, *37*, 179 and 190. [b] This quantity is taken from Table III.

Table V. ΔE_p Values for the Couple $Cp_2Ru_2(\mu\text{-cyclo-}C_8H_8) \rightleftharpoons [Cp_2Ru_2(\mu\text{-cat-}C_8H_8)]^{2+} \rightleftharpoons + 2e^-$ in DMSO/0.1 M Bu_4NPF_6[a]

T (K)	obsd ΔE_p (mV)	theoretical ΔE_p (mV)
383	42	39
363	50	37
343	70	35
293	230	30

[a] v = 0.2 V s^{-1}, Pt electrode. Theory refers to predicted value for Nernstian system.

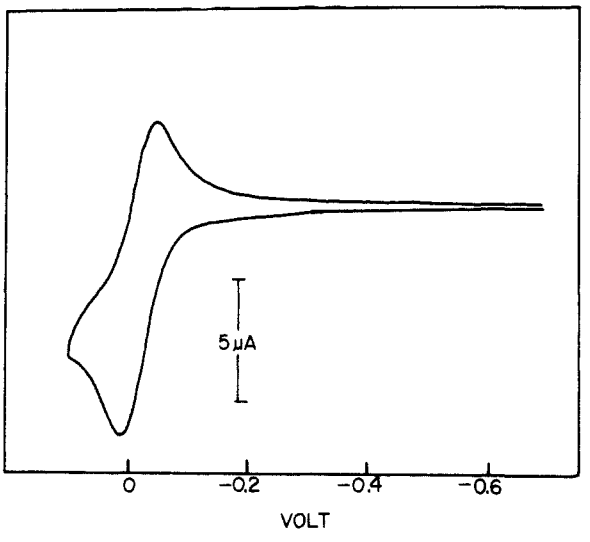

Figure 6. CV of 1.05 mM **1** in DMSO/Bu_4NPF_6 at 360 K, scan rate 0.2 V/s, Pt electrode, Ag/AgCl reference.

of the isomerization reactions. When $T > 370$ K, the ΔE_p values approached those of a Nernstian charge-transfer system (Table V), e.g., at 383 K, theory for fast two-electron transfer = 39 mV, experiment = 42 mV. At these temperatures the waves became qualitatively indistinguishable from those of reversible couples in which no rearrangements take place (Figure 6). This behavior demonstrates quite dramatically the facility with which the electron-transfer-induced ring opening and closing occurs.

II. NMR Spectra. A. The Flyover Complex 2. Complex **2** was first identified by its NMR spectra. The proton spectrum in acetone-d_6 exhibits a singlet Cp resonance and four multiplets for the bridging C_8H_8 group (Table VI). There are two intriguing

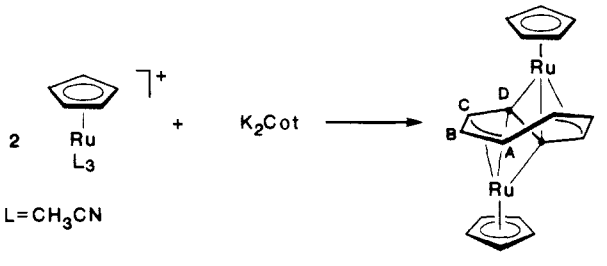

features of the latter: the unusually high chemical shift of one resonance (13.2 ppm) and the fact that two resonances exhibit

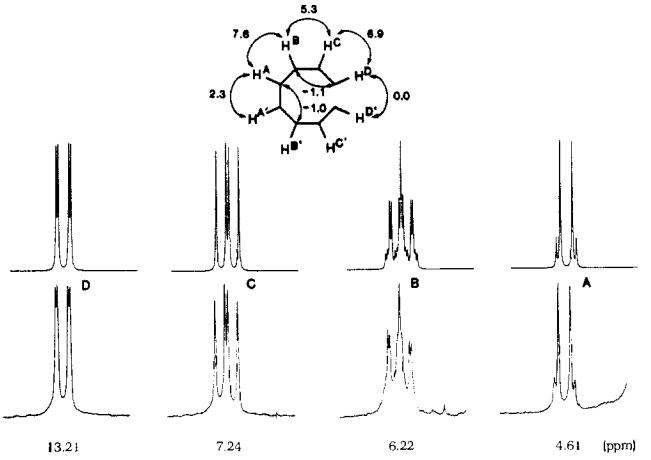

Figure 7. Experimental (lower) and simulated (upper) line patterns of the AA'BB'CC'DD' spin system of the olefinic protons of **2**. The matched coupling constants and their assignments are given in the drawing scheme.

Table VI. NMR Data for $Cp_2Ru_2(\mu\text{-cyclo-}C_8H_8)$, **1**, and $[Cp_2Ru_2(\mu\text{-cat-}C_8H_8)]^{2+}$, **2**[a]

complex	Cp	C_8H_8 (A)	C_8H_8 (B)	C_8H_8 (C)	C_8H_8 (D)
		^1H Spectra (δ)			
1 (CD_2Cl_2, 253 K)	4.51	3.68	4.63	6.21	3.02
2 (C_3D_6O, 298 K)	5.87	4.61	6.22	7.24	13.21
		^{13}C Spectra			
1 (C_6D_6, 296 K)	76.7	66.8	71.5	87.6	42.0
2 (C_3D_6O, 298 K)	92.6	73.6	96.5	91.2	195.3
		^1H–^{13}C Coupling Constants (Hz)			
2 (C_2D_6O, 298 K)	186.7	169.5	171.6	179.9	176.0

[a] Chemical Shifts in δ (ppm), coupling constants in Hz.

first-order splittings, unusual for a theoretical AA'BB'CC'DD' olefinic spin system. ^{13}C spectra were recorded by selective irradiation of individual pairs of protons in order to obtain a complete set of ^{13}C–^1H assignments. The carbon atom associated with the high-frequency proton was found in the ^{13}C spectrum also at a distinctly higher frequency (195.3 ppm) than the other carbon, the shifts of which are in the expected range for metal-complexed sp^2-carbon atoms.

A complete simulation of the proton lines was undertaken, and the matched proton–proton coupling constants are shown in Figure 7. Interestingly, the first-order line splittings of two resonances (7.2 and 13.2 ppm) can be rationalized by the loss of a vicinal coupling constant between two protons with an identical environment. This fact strongly implied that H(D) and H(D') were no longer connected, i.e., that the cyclooctatetraene ring had opened. The carbon high frequency resonance is somewhat low for carbene- or allene-type carbons and reminiscent of those observed in other flyover complexes.[3,22]

II.B. Fluxional Behavior of 1. $Cp_2Ru_2(\mu\text{-cyclo-}C_8H_8)$ is dynamic on the NMR time scale at room temperature and exhibits, besides the Cp resonance, four broad proton lines which resolve on cooling into two pseudodoublets and two pseudotriplets. The ^{13}C spectrum also shows four lines attributable to the cyclooctatetraene ring, this pattern being similar to those observed for other pseudo-triple-decker complexes.[23] Each metal atom is bonded to five carbon atoms of the C_8H_8 ring, both metal atoms sharing a two-carbon atom bridge, so that the molecule possesses a C_2 symmetry perpendicular to that bond.

The line shape of the proton signals (Figure 7) enabled us to distinguish the protons close to the symmetry axis (pseudodoublets)

(22) Yamamoto, T.; Garber, A. R.; Wilkinson, J. R.; Boss, C. B.; Streib, W. E.; Todd, L. J. *J. Chem. Soc., Chem. Commun.* **1974**, 325.
(23) Edwin, J.; Geiger, W. E.; Bushweller, C. H. *Organometallics* **1988**, *7*, 1486.

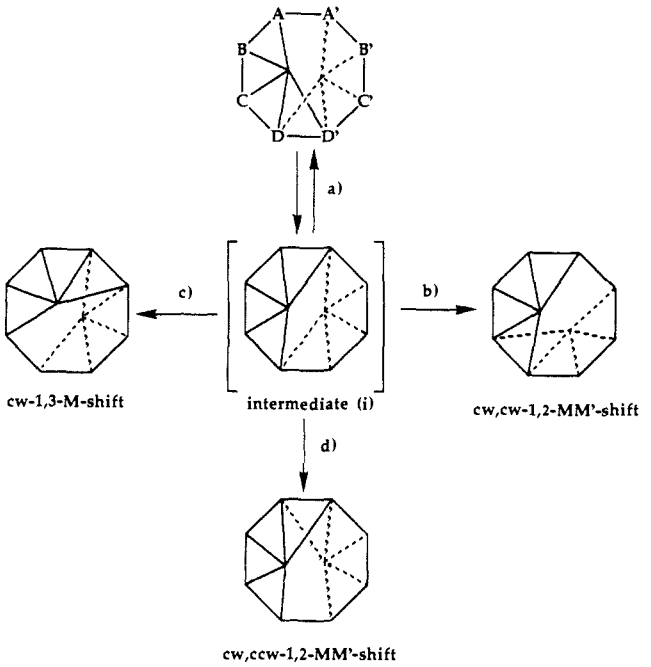

Figure 8. Schematic representation of the four possible rearrangement modes (a)–(d) for complexes of type **1** starting from a common intermediate (i). For explanation see text.

from the remote protons (pseudotriplets). The low-frequency resonance (3.02 ppm, Table VI) was assigned to the bridging carbon atoms, as in an earlier study.[23] Selective irradiation of these protons while recording the ^{13}C spectrum enabled the assignment of C(D) and C(D'). These two atoms (42.0 ppm) are also the most highly shielded carbon atoms, supporting the proton assignment. The assignment of the remaining protons was made by using the spin–spin coupling properties of the vicinal protons. The high-order line shapes required a complete simulation to confirm the connectivity of the CH moieties. The corresponding carbon atoms were assigned as indicated for C(D), C(D'). Final shifts and assignments are collected in Table VI. The proton resonances are all shifted by about −1.6 ppm with respect to those of the isoelectronic complex $Cp_2Rh_2(\mu\text{-}C_8H_8)^{2+}$,[23] owing to the double positive charge on the latter. The close correspondence of the coupling constants between vicinal protons in the two complexes suggests a very similar cyclooctatetraenyl bridge geometry, as was confirmed by the X-ray crystal structures.

On raising the temperature, the pseudodoublets arising from H(A) and H(D) at 3.68 and 3.02 ppm, respectively, broaden faster than the two "triplets" of H(**B**), 4.63 ppm, and H(C), 6.21 ppm. This is what was observed previously for the dirhodium analogue **5**, and in both cases the exchange processes lead to a time-averaged single resonance at the high-temperature limit. Therefore **1** and **5** appear to be subject to the same rearrangement mechanism. The procedure for diagnosing the mechanism is well established,[24] and specific arguments about this type of complex have been previously detailed.[23]

Referring to Figure 8, the most likely rearrangement mechanism for **1** consists of a clockwise 1,3-metal shift of *one* metal or formal conversion of the bonds M–C(D') and M–C(D) to M–C(A') and M–C(B'), respectively (pathway c). The structures in Figure 8 are viewed from the top of one Cp plane. The metal–carbon bonds represented by solid lines are those above the plane of the C_8H_8 ring, and those represented by broken lines are those below the plane. Complex **1** has a higher barrier to rearrangement than does **5**, $\Delta G^{\ddagger}$ = 15.9 kcal/mol vs 14.5 kcal/mol at 320 K. That the lack of positive charge on **1** significantly speeds up the rearrangement suggests that backbonding is an important factor for the transition-state structure. This conclusion ignores possible effects of ion pairing in the dynamic process of **5**.

Since the first-row isoelectronic analogue $Cp_2Co_2(\mu\text{-}C_8H_8)^{2+}$ has a rearrangement mechanism best described as a sequence of clockwise 1,2-metal shifts of *both* metal atoms,[23] one might ask

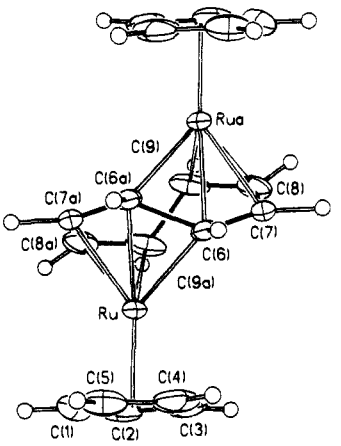

Figure 9. Molecular structure and labeling scheme for **1**, $Cp_2Ru_2(\mu\text{-cyclo-}C_8H_8)$, drawn with 40% probability thermal ellipsoids.

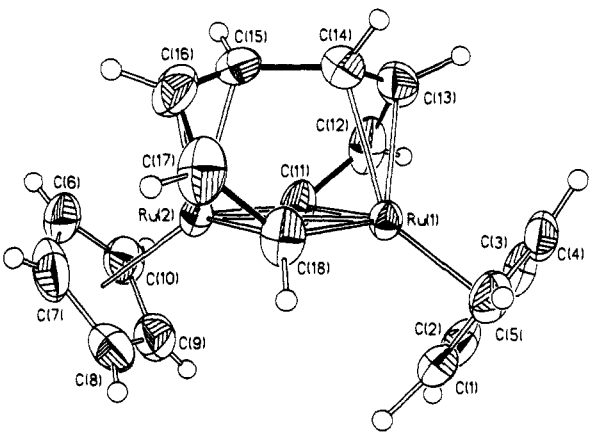

Figure 10. Structure of the dication in **2**, $[Cp_2Ru_2(\mu\text{-cat-}C_8H_8)][PF_6]\cdot 0.5C_6H_6$, drawn with 40% probability thermal ellipsoids.

why these congeners display different behavior. Involvement of a common intermediate [(i, Figure 8] appears to provide a rationalization for these observations. In all cases the first step is a clockwise 1,2-metal shift which converts M–C(D') to M–C–(A'). Then four different routes may be envisioned by which the pseudo-triple-decker structure may be reformed (Figure 8): (Process (a) is not detectable, as it does not involve any net change.) (a) a counterclockwise 1,2-shift of the *same* metal atom; (b) a clockwise 1,2-shift of the *second* metal atom, as observed for the Co complex;[23] (c) a second clockwise shift of the *same* metal atom, giving the overall 1,3-shift observed for **1** and **5**; (d) a counterclockwise shift of the *second* metal atom, which would lead to unselective broadening of all resonances, a process not observed to date in any of these complexes.

For these different rearrangement routes to have different activation barriers, it must be assumed that the intermediate (i) has no mirror plane of symmetry.

III. Structural Considerations. Compound **1** (Figure 9) is isostructural with the previously characterized pseudo-triple-decker complex[11] $[Cp_2Rh_2(\mu\text{-}C_8H_8)]^{2+}$, **5**. The eight-carbon bridging ligand has two planar C_4 moieties [C(16)–C(9), maximum deviation from planarity = 0.002 Å] connected by a dihedral twist of 39.8°. The two C–C bonds connecting the C_4 fragments [C(6) and C(6a); C(9) and C(9a)] are much longer (1.570 (6) and 1.523 (8) Å, respectively) than the other C–C bonds of the cyclooctatetraene ligand (av 1.42 Å). One C–C bond [C(6)–C(6a)] bridges the two metal atoms, each one of these carbon atoms being formally pentavalent.

Complex **2** (Figures 10 and 11) has a structure much like that of the related flyover complex $Cp_2Cr_2(\mu\text{-}C_8H_8)$.[25] A complete

(24) Bennett, M. A.; Bramley, R.; Watt, R. *J. Am. Chem. Soc.* **1969**, *91*, 3089.

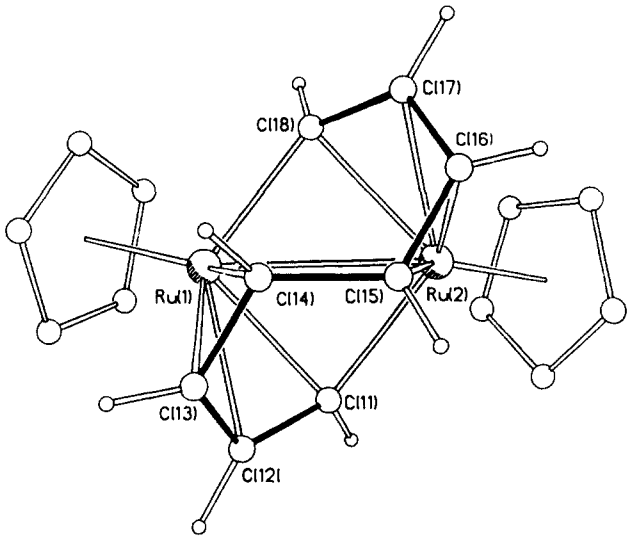

Figure 11. A view of **2** emphasizing the open-chain structure of the C_8H_8 moiety.

set of structural data is available.[26] Each Ru atom is bonded to five carbon atoms and one metal atom, thereby achieving an 18-electron configuration. The longest C–C bond of the eight-carbon linkage is the central bond [C(14)–C(15), 1.491 (7) Å], and the shortest are those adjacent to this bond [C(13)–C(14), 1.400 (8) Å; C(15)–C(16), 1.366 (8) Å]. Other C–C bond lengths fall in the range 1.407–1.417 Å. The two carbon atoms which were formerly bonded in the cyclooctatetraene ring of **1**, C(11) and C(18), are now separated by 3.195 (8) Å. As in **1**, the C_8 group forms two planar units, C(11–14) and C(15–18); the maximum deviation from planarity in each group is 0.057 Å, and the planes are related by a torsional angle of 75.6°.

The view of this complex in Figure 10 emphasizes the planar Ru–C–Ru–C fragment and the carbyne-like bridging of the two ends of the C_8 chain. The bridging carbon atoms are situated asymmetrically between the two metal atoms, with Ru–C distances of 2.131 (4) and 2.066 (4) Å to Ru(1) and 2.063 (4) and 2.143 (5) Å to Ru(2). The closest distance from a metal atom to the hydrogen atom on a bridging carbon atom is over 2.5 Å, too far away to be considered an attractive agostic interaction.

If the solid-state structures of **1** and **2** accurately represent the forms present in solution, then a "least-motion" description of their interconversion may be constructed. In **1** the long C–C bond which uniquely bridges the two metals [C(6)–C(6a), 1.570 (6) Å] probably arises from participation of the two carbon atoms in an electron-deficient, multicentered, bond with the two Ru atoms. If the HOMO contains a bonding contribution from this Ru_2C_2 fragment, rupture of the already weak C–C bond can be rationalized in the monocation of **1**.

This Ru_2C_2 rhombus is preserved on conversion of **1** to **2** in the form of Ru(1)–C(11)–Ru(2)–C(18). During the conversion, the rhombus shifts from acute angles at Ru in **1** [C(6)–Ru–C(6a) = 76.9 (1)°] to obtuse in **2** [av 99.0 (2)°], while the opposite occurs at the rhombus carbon atoms [**1**, Ru–C(6)–Ru(a) = 120.2°; **2**, av Ru–C–Ru = 81.0 (2)°]. Thus, the C(6)–C(6a) bond broken in **1** is replaced by a Ru–Ru bond in **2**.

The reduction of **2** may involve a LUMO with antibonding Ru–Ru character. The M–M distance in **2** [2.7291 (4) Å] is a typical single bond distance for Ru_2. One-electron reduction involving an M–M antibonding orbital would reduce the Ru–Ru bond order to 0.5, but full cleavage and concomitant restoration of the cyclooctatetraene ring would require reduction by a second electron.

IV. Comparison with other Systems Undergoing Ligand Cyclizations. Thermally induced cyclizations of unsaturated flyover chains have been known for many years.[27] Most relevant to our diruthenium results is the interesting thermal isomerization of the open C_8H_8 ligand in $Cp_2Cr_2(\mu\text{-cat-}C_8H_8)$ to $Cp_2Cr_2(\mu\text{-cyclo-}C_8H_8)$, **3** → **4**, vide ante. This reaction[25] contrasts with the Ru_2 results in that the two metals reside on the same face of the cyclooctatetraene ring in the Cr-cyclized product. Linkage of the C_8 chain is postulated to occur through an excited state triplet of the *catena* complex[8] in which there is a less bonding M–M interaction. Cyclization is quite slow (170 h at 423 K) and irreversible.

Two recent studies have reported electron-transfer-induced cyclizations of flyover bridges, albeit in irreversible reactions leading to fragmentation of the complexes. Thus, Robinson, Simpson, and co-workers have detected the anion radical of hexakis(trifluoromethyl)benzene as a major product from decomposition of the anion $\{Co_2(CO)_4[\mu\text{-}C_6(CF_3)_6]\}^-$.[28] Similarly, the diiron complex $Fe_2(CO)_6[\mu\text{-}C_5Ph_4O]$ releases an anion of the cyclized ligand, tetraphenylcyclopentadienone, upon reduction.[29] A likely reason for the observed fragmentations is that the π complexes of cyclized ligands with two metals are less stable when the ring is six-membered than when it is eight-membered.

V. Relation of Observations to Catalyst Mechanisms. Wilke has emphasized that changes in formal metal oxidation state occur when metallacycles are intermediates in metal-catalyzed cyclization reactions of alkynes or olefins,[2] with the reactions being analogous to those of the two-electron redox system of eqs 20 and 21. In this model, formation of the metallacycle (eq 20) from

$$L_mM^n + x\text{alkyne} \longrightarrow \overset{C_{2x}}{\frown}M^{n+2}L_{m-2} \quad \text{oxidative addn} \quad (20)$$

$$\overset{C_{2x}}{\frown}M^{n+2}L_{m-2} \longrightarrow (\pi\text{-}C_{2x}H_{2x})M^nL_{m-2} \quad \text{reductive elim} \quad (21)$$

a metal in a low oxidation state represents an oxidative addition reaction, and the ring-coupling process (eq 21) is a reductive elimination reaction. The aforementioned isomerization of $Cp_2Cr_2(\mu\text{-cat-}C_8H_8)$ to $Cp_2Cr_2(\mu\text{-cyclo-}C_8H_8)$ is a reductive elimination reaction, resulting in a change of chromium oxidation states from $Cr^{II}Cr^{II}$ to $Cr^{I}Cr^{I}$.

The diruthenium complexes display reversible examples of both eqs 20 and 21. Oxidation of $Cp_2Ru_2(\mu\text{-cyclo-}C_8H_8)$ is an oxidatively induced oxidative addition reaction, since the formal metal oxidation states go from Ru^IRu^I in **1** to $Ru^{III}Ru^{III}$ in **2**. Conversely, the back reaction (**2** → **1**) may be viewed as a reductively induced reductive elimination reaction (eq 22).

$$Cp_2Ru_2(\mu\text{-cyclo-}C_8H_8) \underset{\text{red elim}}{\overset{\text{ox addn}}{\rightleftharpoons}} [Cp_2Ru_2(\mu\text{-cat-}C_8H_8)]^{2+} + 2e^- \quad (22)$$

VI. Electron Count Structure Relationship of Pseudo-Triple Deckers. Our group's interest in the electron-transfer properties of the class of complexes $Cp_2M_2(\mu\text{-}C_8H_8)$ had its origin in the theoretical paper by Hoffmann et al.[30] on the electronic and molecular structures of triple-decker sandwich complexes. These authors noted that $Cp_2Co_2(\mu\text{-}C_8H_8)$ has the proper number of metal atoms and π-ligands but the incorrect number of valence electrons (36 e^-) for formation of a true triple-decker complex. It was therefore dubbed a "near-miss" triple-decker.[30] The present paper and its companion (the preceding article in this issue), together with earlier preliminary communications,[11,16] allow a relatively complete picture to be drawn of the effect of removal of electrons on the structure of pseudo-triple-decker complexes, from the 36 e^- complexes down to the formal 32-electron complex **2**, at least when the two metals reside on the *opposite* faces of

(25) Geibel, W.; Wilke, G.; Goddard, R.; Kruger, C.; Mynott, R. *J. Organomet. Chem.* **1978**, *160*, 139.
(26) Supplementary material from ref 9.

(27) Mills, O. S.; Robinson, G. *Proc. Chem. Soc.* **1964**, 187, personal communication to Hoogzand, C. and Hubel, W., quoted in ref 2, p 685.
(28) Arewgoda, C. M.; Bond, A. M.; Dickson, R. S.; Mann, T. F.; Moir, J. E.; Rieger, P. H.; Robinson, B. H.; Simpson, J. *Organometallics* **1985**, *4*, 1077.
(29) Osella, D.; Botta, M.; Gobetto, R.; Laschi, F.; Zanello, P. *Organometallics* **1988**, *7*, 283.
(30) Lauher, J. W.; Elian, M.; Summerville, R. H.; Hoffmann, R. *J. Am. Chem. Soc.* **1976**, *98*, 3219.

Scheme II

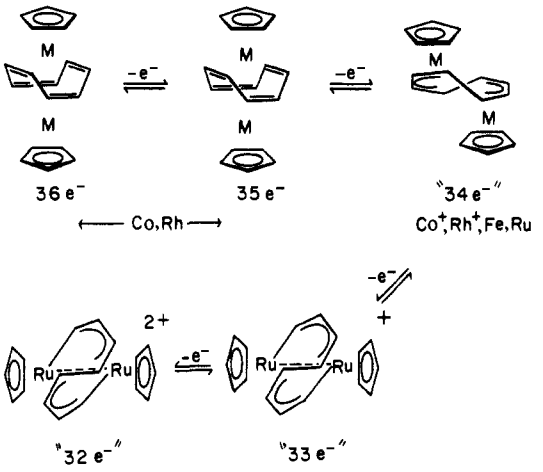

the C_8 ring. Scheme II summarizes the known structural preferences.

The thermodynamically favored structures are given in each case with the structure of the 35 e^- species being the only one in serious question. The question mark for the 35 e^- species relates to uncertainty of whether the observation of the tub form of $[Cp_2Rh_2(\mu\text{-}C_8H_8)]^+$ (see preceding paper in this issue) has its origin in the kinetic or thermodynamic preference of the 35 e^- species.

Note that the formal electron count in this scheme is derived employing a constant number of valence electrons for both the C_8H_8 ligand (8 e^-) and the CpM moieties (14 e^- for CpRh, 13 e^- for CpRu). This emphasizes the electron-deficient nature of the metals in the 34 e^- and 32 e^- species. However, the metals form new bonds after each two-electron transfer, thereby retaining the 18 e^- structure in each even-electron species. Thus, when the "34 e^-" species is formed, the bridging C–C bond of the cyclooctatetraene ligand donates an extra electron to each metal, thereby achieving coordinative saturation. Similarly, M–M bond formation provides another valence electron to each metal in the "32 e^-" species. In simple terms, then, the stability of the 18 e^- configuration for each metal provides a rationalization of the even-electron structures of the entire series.

Acknowledgment. W.E.G. gratefully acknowledges the support of this research by the National Science Foundation (CHE86-03728). A.S. and W.v.P. thank the Swiss National Science Foundation for Grants 20-5406.87 and 2000-4.933.

Experimental Study of HCN^+ and HNC^+ Ion Chemistry

Simon Petrie, Colin G. Freeman, Michael Meot-Ner (Mautner), Murray J. McEwan,* and Eldon E. Ferguson†

Contribution from the Department of Chemistry, University of Canterbury, Christchurch, New Zealand. *Received August 16, 1989. Revised Manuscript Received May 2, 1990*

Abstract: We report the results of a room temperature selected ion flow tube study of reactions of HCN^+ and HNC^+. Electron impact on HCN was found to produce a mixture of HCN^+ and HNC^+ isomers. HCN^+ was found to be isomerized efficiently to HNC^+ by reaction with CO or with CO_2, and isomerization is expected to occur for any other species M having a proton affinity PA(CN at C) < PA(M) < PA(CN at N). The isomerization process is interpreted in terms of a "forth and back" proton transfer mechanism. A monitor gas technique was used to distinguish between the isomers. With CF_4, HCN^+ was reactive ($k = 1.2 \times 10^{-9}$ cm^3 s^{-1}) and HNC^+ unreactive. With SF_6 both isomers react at the collision rate but HCN^+ yields only SF_5^+ as the product ion whereas HNC^+ yields only $HNCF^+$. Thermodynamic data established in this work include $\Delta H_f(HNC^+) \leq 1373$ kJ mol^{-1}, and hence PA(CN at N) ≥ 595 kJ mol^{-1}.

Introduction

The present investigation is a continuation of the study of isomeric ion chemistry involving small ions of astrophysical interest carried out recently in this laboratory. Previous studies, utilizing the selected ion flow tube (SIFT) technique, have involved CH_3CNH^+/CH_3NCH^+,[1] HCO^+/HOC^+,[2] and CNC^+/CCN^+[3] isomers. Other groups that have examined isomeric structures in flow tubes include Smith and Adams[4] and Bohme et al.[5] The reactions are measured in a flow tube with mass spectrometric detection. The identical mass isomeric ions are distinguished on the basis of their different reactivities with selected neutrals. This variation of the so-called "monitor ion" technique involves the addition of a neutral monitor reactant gas prior to mass analysis. In an ideal situation, the reaction of the monitor gas is exothermic and fast with the most energetic isomer and endothermic and does not occur with the more stable isomer. However, different isomeric forms have been distinguished when both isomers react, but at very different rates. The monitor ion technique was first used in Flowing Afterglows to distinguish electronically excited metastable ions from ground-state ions in order to study the reactivities of electronically excited ions.[6] Recently the monitor ion technique has been utilized to distinguish between ions in different vibrational states in order to measure collisional[7] and radiative[8] ion vibrational relaxation.

In the present study two suitable monitors were found that enable HCN^+ and HNC^+ to be readily distinguished in a flow

† Permanent address: NOAA, Climate Monitoring and Diagnostics Lab, 325 Broadway, Boulder, CO 80303-3328. Visiting Erskine Fellow at Canterbury, 1989.

(1) Knight, J. S.; Freeman, C. G.; McEwan, M. J. *J. Am. Chem. Soc.* **1986**, *108*, 1404.
(2) Freeman, C. G.; Knight, J. S.; Love, J. G.; McEwan, M. J. *Int. J. Mass Spectrom. Ion Proc.* **1987**, *80*, 255.
(3) Knight, J. S.; Petrie, S. A. H.; Freeman, C. G.; McEwan, M. J.; McLean, A. D.; DeFrees, D. J. *J. Am. Chem. Soc.* **1988**, *110*, 5286.
(4) Smith, D.; Adams, N. G. *Int. J. Mass Spectrom. Ion Proc.* **1987**, *76*, 307.
(5) Bohme, D. K.; Wlodek, S.; Raksit, A. B.; Schiff, H. I.; Mackay, G. I.; Keskinen, K. J. *Int. J. Mass Spectrom. Ion Proc.* **1987**, *81*, 123.
(6) Lindinger, W.; Albritton, D. L.; McFarland, M.; Fehsenfeld, F. C.; Schmeltekopf, A. L.; Ferguson, E. E. *J. Chem. Phys.* **1975**, *62*, 4101.
(7) Böhringer, H.; Durup-Ferguson, M.; Fahey, D. W.; Fehsenfeld, F. C.; Ferguson, E. E. *J. Chem. Phys.* **1983**, *79*, 4201.
(8) Heninger, M.; Fenistein, S.; Durup-Ferguson, M.; Ferguson, E. E.; Marx, R.; Mauclaire, G. *Chem. Phys. Lett.* **1986**, *131*, 439.

0002-7863/90/1512-7121$02.50/0